Theme Number(s): XX

Static and Seismic Assessment of Soil Arching in a Piled Embankment

Sanjay Nimbalkar[1*][0000-0002-1538-3396] and Naveen Kumar Meena[1][0000-0001-9678-0950]

[1]School of Civil and Environmental Engineering, University of Technology Sydney, NSW 2007 Australia
[*]Sanjay.Nimbalkar@uts.edu.au

Abstract: Piled embankments are widely used to improve the weak soil characteristics and elevate the ground level for the construction of transport corridors on the weak soil. These embankments allow fast construction and a significant reduction in differential settlement. In the pile-supported railway embankment, most of the imposed load is transferred to the rigid pile through a shearing stress mechanism named as "soil arching". Several studies contribute to the assessment of soil arching under static loading. However, studies dealing with the effect of the seismic excitation on soil arching in pile-supported railway embankment are scarce. The present study is focused on addressing the effects of static loading and seismic excitation using Finite Element Analysis (FEA) in Two-dimensional (2D) state of stress. The FEA results indicate that piled embankment properties such as friction angle, pile and embankment fill modulus should be improved for the efficient mobilization of soil arching. The arching zone is influenced by varying the pile spacing. In addition, the available design approach shows a variation with numerical results. The soil arching is poorly developed indicating insufficient mobilization under the seismic excitation. This in turn results in the transfer of higher stresses to soft soil. The present study thus presents the detrimental effects of earthquake on transport infrastructure projects constructed in soft soil regions.

Keywords: Finite element analysis, Piled embankment, Soil arching, Earthquake.

Notations and Abbreviations

Notations

[C]	Damping matrix (dimensionless)
[M]	Mass matrix (dimensionless)
[K']	Stiffness matrix (dimensionless)
ξ_0	Damping ratio (dimensionless)
ω_i and ω_j	Natural frequency (Hz)
α and β	Damping coefficients (kNs/m)
λ	Logarithmic hardening constant (dimensionless)

γ	Unit weight (kN/m^3)
ϕ	Dynamic amplification factor (dimensionless)
v	Poisson's ratio (dimensionless)
ψ	Dilation angle (degree)
ϕ'	Friction angle (degree)
c'	Cohesion (kPa)
p_o'	Effective overburden pressure (kPa)
σ_h	Horizontal stress (kPa)
σ_p	Vertical stress on pile (kPa)
σ_s	Vertical stress on subsoil (kPa)
σ_v	Vertical stress (kPa)
E_{em}	Embankment modulus (MPa)
E_p	Pile modulus (GPa)
F_d	Design equivalent dynamic load (kN)
F_s	Static wheel load (kN)
K_o	Lateral stress coefficient at rest state (dimensionless)
K_p	Lateral stress coefficient at passive state (dimensionless)
N_{em}	Normalized embankment height (dimensionless)
N_{vs}	Normalized vertical stress (dimensionless)
P_{es}	Plane of equal settlement (m)
a_o	Initial yield surface size (kPa)
e_o	Initial void ratio (kNs/m^2)
e_1	Void ratio at unit pressure (kNs/m^2)
D	Pile diameter (m)
E	Modulus of elasticity (MPa)
K	Lateral stress coefficient (dimensionless)
M	Critical-state stress ratio (dimensionless)
SAR	Soil arching ratio (dimensionless)
d	Pile wall width (m)
h	Embankment height (m)
k	Logarithmic bulk modulus (kPa)
q	Surcharge on the embankment top (kN)
s	Pile spacing (m)
a, b, c, a', b' and c'	Relationship constant (dimensionless)

Abbreviations

2D	Two-dimensional
3D	Three-dimensional
CINPE4	Four-node plane strain linear infinite element
CPE8R	Eight-node plane strain element with reduced integration
EA	Equivalent Area
FEA	Finite Element Analysis
MC	Mohr-Coulomb
MCC	Modified Cam Clay
ORE	Office of Research and Experiments
PGA	Peak ground acceleration

1 Introduction

Across the globe, increase in population and demand of associated roads, railways and public transport infrastructure has stimulated professionals to use soft compressible soils, which otherwise deemed conventionally unsuitable foundation material. Since, the weak soil has less bearing capacity and high compressibility, piled embankment is often used as a suitable engineering alternative providing benefits in terms of rapid construction, lesser differential settlement and elevating the ground level for construction of transport corridors on such weak soils.

In the pile-supported railway embankment, most of the imposed load is transferred to the rigid pile through a shearing stress mechanism named as soil arching [1]. In the recent decade, several studies [2-5] focused on the mechanism of soil arching. Han and Gabr [2] performed numerical investigations to assess the soil arching by considering three major influence factors: the height of the fill, the tensile stiffness of geosynthetic, and the pile elastic modulus under static loading condition. They reported that soil arching is significantly affected by the variation in piled embankment properties. A case study of pile-supported transport embankment is reported by Liu et al. [3]. The case history was back analyzed in finite element analysis and authors concluded that significant load was transferred on the pile top due to the soil arching. Wu et al. [4] reported a full-scale experiment to investigate the performance of piled embankment. A numerical analysis was also performed in two-dimensional (2D) plane strain condition to compare applicability of the different numerical approaches. The numerical model adopting Equivalent Area (EA) approach was in good agreement with experimental results. In addition, Modified Cam Clay (MCC) soil constitutive model yielded good prediction with the experimental results. Almeida et al. [5] performed numerical and analytical modeling of a series of centrifuge tests. A static surcharge was considered on the embankment top. The Numerical results yielded good agreement with European guidelines.

Most of the past studies investigated soil arching under the static loading condition on the piled embankment. Due to traffic loading and seismic excitation, the complex behavior of soil arching in the pile-supported railway embankment is largely unknown. Heitz et al. [6] reported model tests to investigate the vertical stress distribution on the pile and subsoil under the cyclic loading. Lehn et al. [7] conduced a three-dimensional (3D) numerical simulation under the cyclic loading and observed that the soil arching was stable upto 50 cycles of load. As per the writers' best knowledge, there is no study yet to be reported which deal with the investigation of the seismic assessment of soil arching under a pile-supported railway embankment.

In the present book chapter, the results of Finite Element Analysis (FEA) focusing on the static and seismic assessment of soil arching in a pile-supported railway embankment are presented and discussed. This chapter also identifies the key input parameters of the piled embankment which are found to largely affect the mobilization of soil arching.

2 Finite element analysis

The finite element based commercial software ABAQUS 2018 [8] is used to assess the soil arching under the static loading and earthquake condition. The key points of the FEA such as analyzed area, soil constitutive model, mesh size, element type, interface, boundary condition, loading and modeling procedure are illustrated in this section.

2.1 General description

A series of FEA simulations are carried out to assess the soil arching in the 2D plane strain condition. The 2D modelling requires less computational facility and time needed for simulation. The central part of a pile-supported railway embankment considered for the numerical simulation. The embankment height (h), pile spacing (s) and diameter (D) are chosen as 3.5 m to 6.5 m, 2 m to 3.5 m and 1 m, respectively. Pile length and subsoil depth are chosen same as 8 m. A typical schematic diagram of modelled unit cell is shown in Fig. 1.

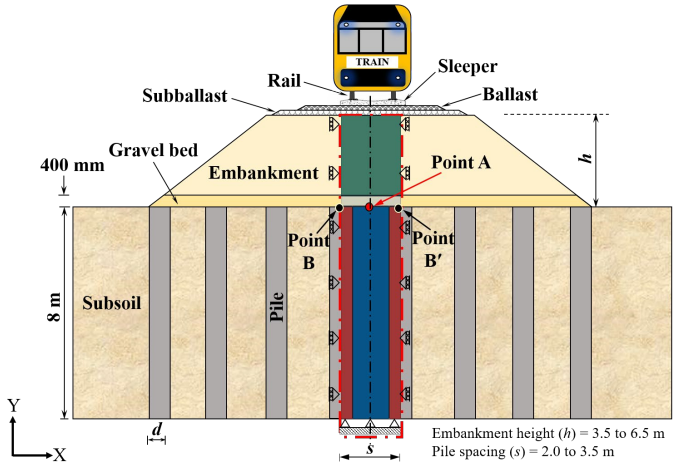

Fig. 1. A typical pile-supported railway embankment with modelled unit cell (modified from Meena et al. [9])

Various methods have been reported in the past which report the conversion of a 3D piled embankment into 2D and it is argued that Equivalent Area (EA) method is in good agreement with the 3D model [4, 10]. Area replacement ratio of the pile to surrounding soil in both 3D and 2D is preserved in the EA method. Whereas in other methods, pile wall thickness is kept same with equivalent elastic modulus considering the normal and flexural stiffness of pile. The pile arrangement is assumed in square pattern (i.e., s_x and $s_y = s$). The principle of the EA method to convert a pile diameter into the equivalent wall is explained in Fig. 2.

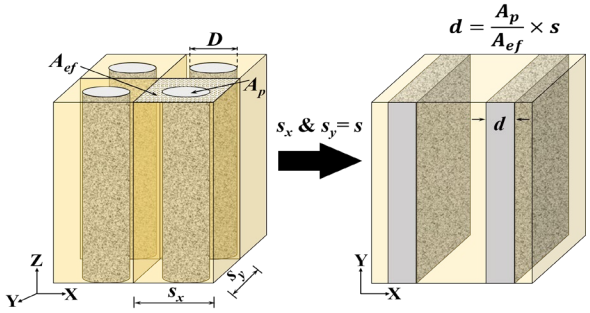

Fig. 2. Typical illustration of the principle of EA method (modified from Zhang et al. [10])

2.2 Boundary condition, mesh size, element type, interface and seismic input

Vertical boundaries of the numerical model are laterally restrained, while the base boundary is fully fixed. The adoption of infinite element boundary can reduce the wave reflection from the model boundaries during the seismic analysis. The FEA results can be affected by the element type and mesh size. The eight-node plane strain element with reduced integration (CPE8R) is used for this study. The four-node plane strain linear infinite element (CINPE4) is used for infinite boundary under the seismic analysis [11]. In addition, the interaction between the pile and surrounding soil is stimulated using basic coulomb friction model [12]. The mesh size is chosen according to the master and slave surface criteria.

The seismic input of Christchurch 2011 earthquake is used for the seismic assessment of the soil arching [13]. The magnitude of this earthquake on Richter scale is 6.3 M_L for 30 s time duration. The peak ground acceleration (PGA) is taken as 0.34g. The seismic parameters of the Christchurch 2011 earthquake are similar with a few major Australian earthquakes as summarized in Table 1.

Table 1. A few major earthquakes in Australian territories (data sourced from [14])

Year	States of Australia	Earthquake magnitude (M_L)	Peak ground acceleration (PGA)
2016	Northern Territory	6.1	0.49g
1997	Western Australia	6.2	0.50g
1979	Western Australia	6.1	0.20g
1968	Western Australia	6.5	0.20g
1941	Western Australia	6.3	0.20g

2.3 Soil constitutive model and material damping

An appropriate constitutive model of soil in FEA is necessary to achieve the precise results. The Mohr-Coulomb (MC) model is commonly used for granular material such as embankment fill and gravel bed. The Modified Cam Clay (MCC) is well recognized for describing the behavior of soft compressible soil such as clay. The material

damping is essential characteristics of the seismic analysis. The Rayleigh damping is commonly used for the seismic analysis in finite elements and it is expressed as [15]:

$$[C] = \alpha[M] + \beta[K'] \tag{1}$$

where, [C] is damping matrix, [M] is mass matrix, [K'] is stiffness matrix, α and β are the damping coefficients calculated as:

$$\alpha = 2 \times \left(\frac{\omega_i.\omega_j}{\omega_i+\omega_j}\right) \times \xi_0 \tag{2}$$

$$\beta = \left(\frac{2}{\omega_i+\omega_j}\right) \times \xi_0 \tag{3}$$

The ω_i and ω_j are natural frequencies of the model and ξ_0 is the damping ratio. In this study, the ω_i and ω_j are computed by model analysis. The damping ratio is considered as 3 %. From Eqs. 2 and 3, the damping coefficients α and β are calculated as 0.032 and 0.0017.

All the material properties are summarized in Table 2. This study is performed assuming the fully drained condition consequently the development of excess pore water pressure is neglected. For the subsoil simulated as MCC material, initial yield surface size (a_o) is calculated as [3]:

$$a_o = \frac{1}{2}\exp[\frac{(1+e_o)(e_1-e_o.k.lnp_o')}{(\lambda-k)}] \tag{4}$$

where, e_o is initial void ratio; e_1 is void ratio at unit pressure; k is logarithmic bulk modulus; p_o' is effective overburden pressure and λ is logarithmic hardening constant.

Table 2. Material properties used in FEA [3, 9]

Material properties	**Embankment fill**	**Gravel bed**	**Subsoil**
Constitutive model	MC	MC	MCC
Unit weight, γ (kN/m^3)	20	21	19.7
Young's modulus, E (MPa)	20	25	-
Poisson's ratio, v	0.25	0.25	0.35
Effective cohesion c′ (kPa)	0.1	0.1	-
Effective friction angle, ϕ' (degree)	30	35	-
Effective dilation angle, ψ (degree)	0	5	-
Critical-state stress ratio, M	-	-	1.2
Logarithmic hardening constant, λ	-	-	0.06
Logarithmic bulk modulus, k	-	-	0.012

Initial yield surface size, a_o (kPa)	-	-	103*
Void ratio at unit pressure, e_1	-	-	0.87
Initial void ratio, e_o	-	-	0.45

Note: * calculated from Equation (4)

2.4 Loading on the embankment top

In this study, an equivalent dynamic load is applied on the top of the modeled unit cell to mimic the load of rail track with moving train. The equivalent dynamic load is defined as [16, 17]:

$$F_d = \phi . F_s \tag{5}$$

where, F_d is design equivalent dynamic load (kN); ϕ is dynamic amplification factor (dimensionless) and F_s is static wheel load (kN). Office of Research and Experiments (ORE) and 2:1 methods are adopted to calculate the ϕ and equivalent dynamic load on the embankment top, respectively. In this study, heavy haul freight train with axle load of 35 tone moving at a speed of 40 km/h is considered. For more details on the variation in train induced dynamic loads against the nominal range of train speeds (40 to 160 km/h) is provided in Table 3. The details of equivalent dynamic load on the embankment top are summarized in Table 3.

Table 3. Train induced equivalent dynamic load on the embankment top (data sourced from [9])

Train speed, V (km/h)	**Static wheel load, F_s (kN)**	**Dynamic amplification factor, ϕ**	**Equivalent dynamic load, F_d (kN)**
40	81.23	1.29	105
80	81.65	1.31	107
120	80.94	1.36	110
160	81.17	1.45	118

2.5 Modeling procedure

First, initial stress and predefined void ratio are established in the subsoil considering geostatic step. Construction stages of embankment including the gravel bed are processed followed by the insertion of rigid piles. After achieving full embankment height in 4 days, an equivalent dynamic load of railways track including the moving train is imposed on the embankment top. Subsequently, seismic excitation appropriate to the Christchurch 2011 earthquake is applied on the bottom of model adopting the dynamic implicit stepping scheme.

3 Results and discussions

3.1 Vertical stress distribution in the embankment fill

The soil arching can be assessed in terms of the vertical stress distribution from the embankment top to base at point A (refer Fig. 1). Fig. 3 and 4 show the vertical stress distribution in the embankment fill over point A. The vertical stress and embankment height are normalized for the sake of general applicability. The effect of embankment height (h) and pile spacing (s) is shown in Fig. 3 and 4, respectively. The pile spacing (s) is taken 2.5 m to investigate the effect of embankment height on the soil arching. It is evident from Fig. 3 that normalized vertical stress ($N_{vs} = \sigma_s/\{\gamma.(s\text{-}d)\}$) follows the depth-wise linearly increasing trend of geostatic stress from the embankment top to the depth attaining 1.5 fold normalized embankment height ($N_{em} = h/(s\text{-}d)$). This embankment height represents the outer boundary of soil arching for all considered embankment height (i.e., 3.5 m, 5.0 m and 6.5 m). Below this outer boundary, the N_{vs} shows decrease up to the $0.4\times N_{em}$ which is represented as the inner boundary of soil arching. The vertical depth located between the upper and inner boundaries of soil arching can be defined as soil arching zone and the majority of vertical stress is transferred to the pile top (on point B or B′) at the inner boundary of soil arching. The N_{vs} again increases following the linearly increasing trend due to the self-weight of embankment fill underneath the inner boundary of soil arching. The same trend of vertical stress on subsoil has been observed elsewhere in the literature [3]. It is worth noting that the soil arching zone is not effected by the embankment height.

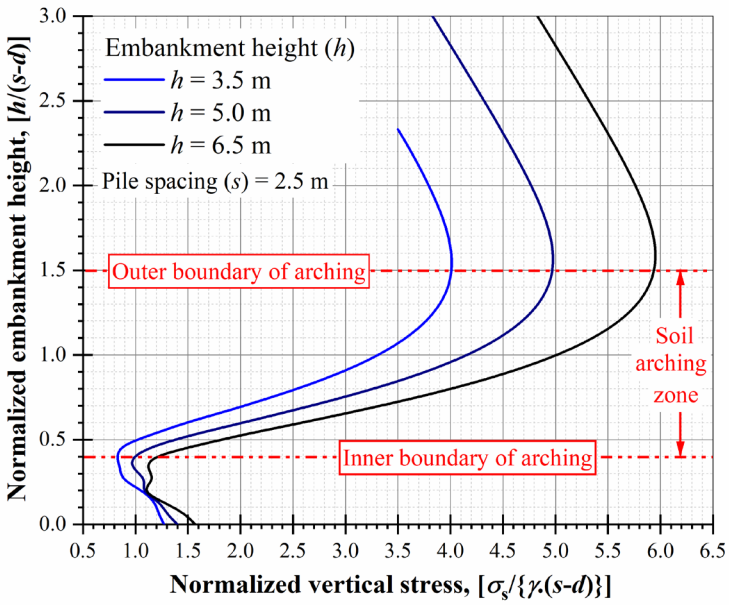

Fig. 3. Vertical stress over the point A in embankment fill for different embankment height

In Fig. 4, the embankment height (h) is chosen 3.5 m and it is evident that for the given range of pile spacing, the N_{vs} trend follows the same trend as illustrated in Fig. 3. The inner boundary is the same for all pile spacing. However, the upper boundary varies with pile spacing. The upper boundary lies on the $1.9\times N_{em}$, $1.5\times N_{em}$ and $1.3\times N_{em}$ for the pile spacing of 2.0 m, 2.5 m and 3.5 m, respectively. It implies from Fig. 4 that the soil arching zone increases with a decrease in pile spacing. Therefore, it is crucial to provide an optimum pile spacing, allowing for the installation tolerances of rigid piles.

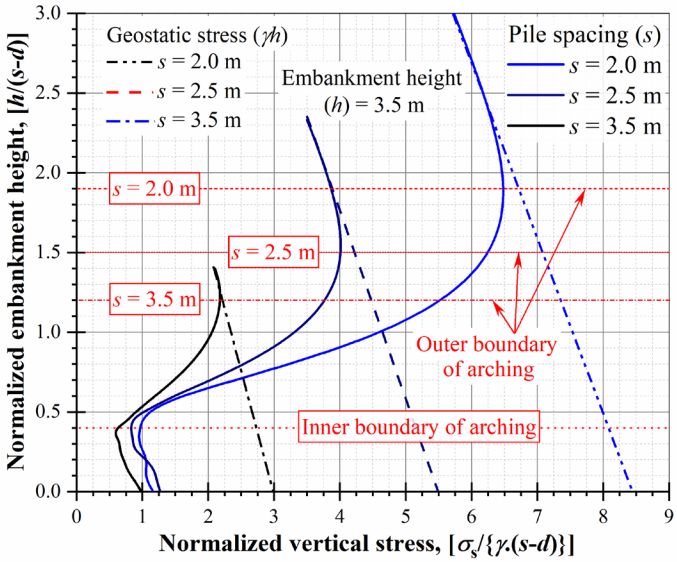

Fig. 4. Vertical stress over the point A in embankment fill for different pile spacing

3.2 Settlement in embankment fill

Settlement of embankment in the piled embankment is a crucial factor from the serviceability aspect. The soil arching can be associated with the serviceability of piled embankment through reduction in settlement of soft soil. Fig. 5 and 6 show the settlement in the embankment-fill over point A and B (or B′) for different embankment height (h) and pile spacing (s). The settlement of embankment fill associated to different embankment heights is shown in Fig. 5. The pile spacing is considered as 2.5 m. It is evident that the settlement on the pile top (point B or B′) is nearly zero for all considered embankment height. However, the settlement on the mid of embankment base (point A) is slightly increased with an increase in embankment height. In addition, uniform settlement on point A and B (or B′) is observed above the $1.9\times N_{em}$ for all considered embankment height. This embankment height is referred as plane of equal settlement (P_{es}) in the literature [18].

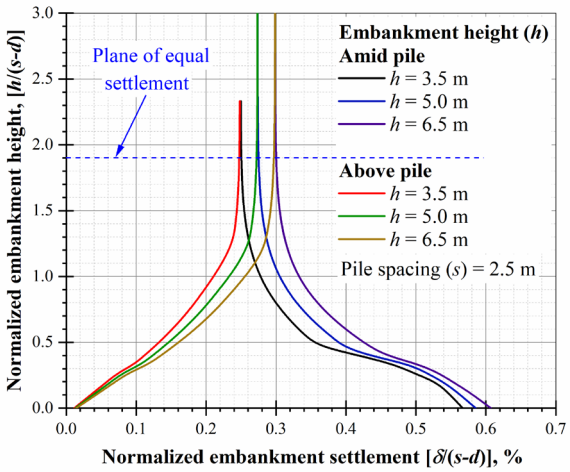

Fig. 5. Settlement over points A and B (or B′) in embankment fill for different embankment height

Effect of the pile spacing on the settlement of embankment fill under the fixed embankment height (i.e., 3.5 m) is shown in Fig. 6. It is observed that for the considered range of pile spacing, the settlement follows the same trend as Fig. 5. However, the P_{es} varies with the pile spacing. The P_{es} occurred at $2.4\times N_{em}$, $1.9\times N_{em}$ for the pile spacing of 2 m and 2.5 m, respectively. The P_{es} does not seem to exist for the pile spacing 3.5 m. From Figs. 4 and 6 it is concluded that the outer boundary of soil arching develops below the P_{es}.

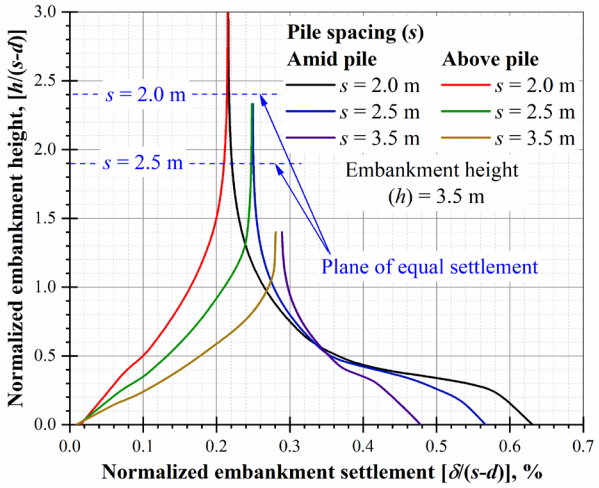

Fig. 6. Settlement over points A and B (or B′) in embankment fill for different pile spacing

3.3 Effect of key parameters of piled embankment on soil arching ratio

The degree of soil arching in a piled embankment can be described by the soil arching ratio (*SAR*). The ratio of vertical stress on point A (σ_s) to geostatic stress including surcharge ($\gamma.h+q$) is known as soil arching ratio [2]:

$$SAR = \frac{\sigma_s}{(\lambda.h+q)} \tag{6}$$

where, σ_s is vertical stress on point A; γ is unit weight of embankment fill; h is embankment height and q is surcharge. The unit value of *SAR* implies no soil arching. While *SAR* = 0 denotes full mobilization of soil arching.

The effect of piled embankment parameters such as pile and embankment modulus, friction and dilation angle on the *SAR* is shown in Figs. 7 and 8. The *SAR* associated with pile and embankment modulus is illustrated in Fig. 7. It shows that the *SAR* decrease up to 25 % with an increase in embankment modulus (E_{em}) from 15 MPa to 30 MPa. However, the pile modulus (E_p) has a negligible effect on the *SAR* due to higher modulus of elasticity of rigid pile. The E_p is considered fixed at 20 GPa for the *SAR* corresponding to the E_{em}. In contrast, the E_{em} is fixed at 20 MPa. The effect of E_{em} on the *SAR* is confirmed in Han and Gabr [2].

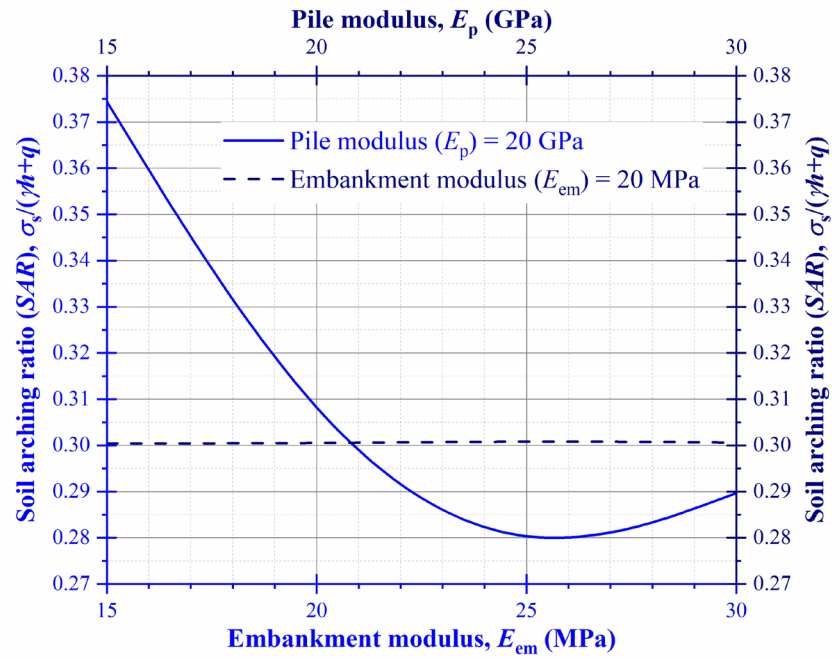

Fig. 7. Effect of pile and embankment modulus on the soil arching ratio

Fig. 8 shows the *SAR* associated with the angles of friction and dilation. It is observed that the *SAR* decreases up to 30 % with an increase in effective friction angle

(ϕ') from 30° to 45°. In addition, the SAR decreases up to 7 % with an increase in dilation angle (ψ) from 0° to 15°. The value of ψ is fixed at 0° for the *SAR* corresponding to the varying ϕ'. In contrast, ϕ' is fixed at 30°. It implies that effective friction angle of embankment fill is an important parameter compared to dilation angle. Thus, Figs. 7 and 8 conclude that the embankment modulus and friction angle is more prominent parameters of the piled embankment and higher values must be maintained for achieving full mobilization of the soil arching.

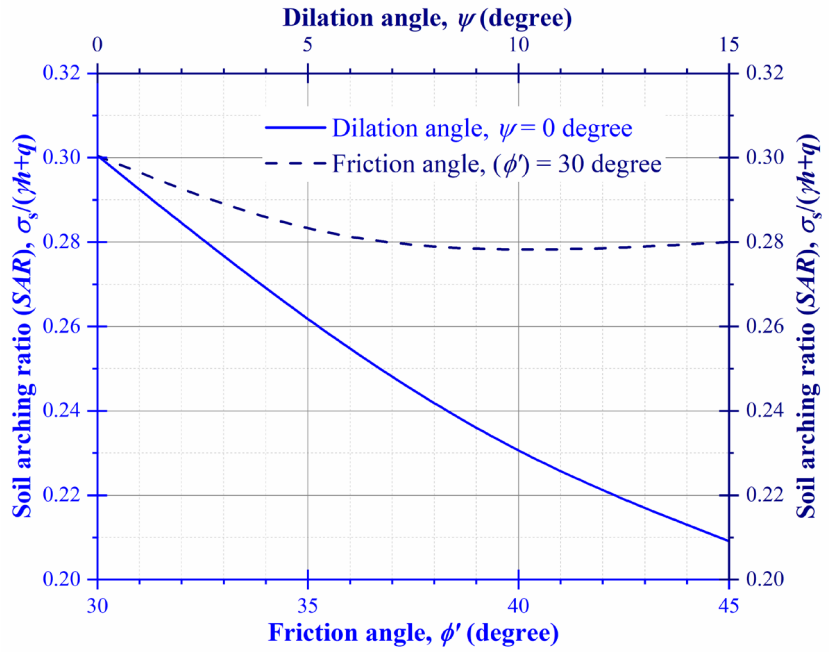

Fig. 8. Effect of friction and dilation angle on the soil arching ratio

3.4 Effect of the earthquake on soil arching

The piled embankment with 3.5 m embankment height and 2.5 m pile spacing is considered to study the effect of earthquake on soil arching. Fig. 9 illustrates the N_{vs} distribution in the embankment fill over point A with and without earthquake condition. In the absence of earthquake, the N_{vs} distribution follows the same trend as shown in Fig. 3. The N_{vs} is consistent with the geostatic stress from the embankment top to 1.5 N_{em}. Subsequently it decreases up to 0.4×N_{em} and beneath this height, the N_{vs} again increases due to the self-weight of embankment fill. In contrast, the N_{vs} consistently increase from the embankment top to bottom during the earthquake. However, a marginal increment of the N_{vs} is observed on the pile top (point B or B′). It implies that soil arching is not mobilized properly under the earthquake condition.

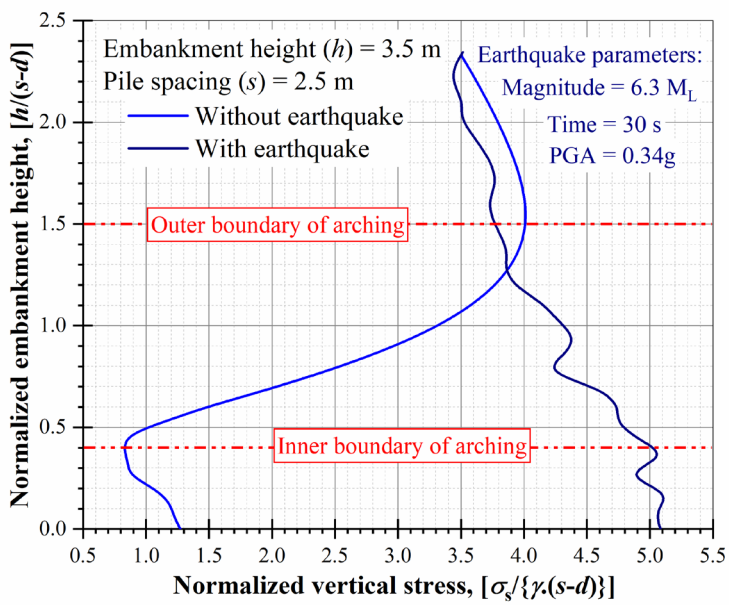

Fig. 9. Effect of earthquake on vertical stress over the point A in embankment fill

Fig. 10 shows the lateral stress coefficient (K) in embankment over the point A with and without earthquake. The lateral stress coefficient is the ratio of horizontal stress (σ_h) to vertical stress (σ_v). In the absence of earthquake, the lateral stress coefficient exists at rest (K_o = 0.5) after the normalized embankment height (N_{em}) of 2.0. This embankment height is referred to as the plane of equal settlement as discussed earlier in Fig. 5. Subsequently the K tends to approach the passive state (K_p = 3.0) at the N_{em} of 0.4, which represent the inner boundary of soil arching as explained in the Fig. 3. In contrast, the K does not follow the same trend during the earthquake. The K remains almost the same (i.e., K = 0.8) throughout the N_{em}. It is worth noting that earthquake disrupts the mobilization of the full soil arching, while achieving the partial soil arching and consequently, the majority of vertical stress is imparted on subsoil (i.e., point A) which in turn could lead to failure.

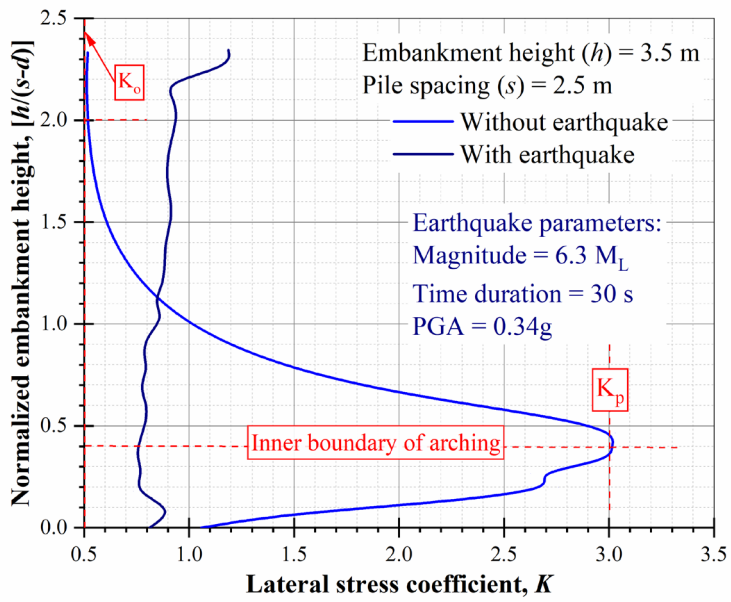

Fig. 10. Effect of earthquake on lateral stress coefficient over the point A in embankment fill

3.5 Review of available design approaches

Three well-established design approaches such as Terzaghi [1], Hewlett and Randolph [19] and BS8006 [20] are used to compare the numerical results. Terzaghi method [1] is based on assumption of equal settlement plane. Terzaghi [1] defined an imaginary soil column in the embankment-fill between vertical slip up to a certain height and this height is referred to as the plane of equal settlement. Consequently, shape of the soil arching is rectangular. Hewlett and Randolph [19] and BS8006 [20] follow the limit equilibrium model. Hewlett and Randolph [19] observed the semicircular arch and a hemispherical dome with uniform thickness corresponding to 2D and 3D conditions. The failure is presumed either on the crown of soil arch (i.e., semicircular arch and a hemispherical dome) or on the pile top. It is confirmed that the pile top is critical area in the plane strain condition while, crown of soil arch is more critical in 3D condition [19]. The failure theory adopted in Hewlett and Randolph [19] is shown in Fig. 11.

The BS8006 [20] altered these empirical model using plane of equal settlement. The BS8006 [20] reported two conditions for soil arching; (i) partial aching, when $0.7\ (s\text{-}D) \leq h \leq 1.4\ (s\text{-}D)$ and (ii) full arching, when $h \geq 1.4\ (s\text{-}D)$. In this chapter, the range of embankment height (h) is taken as 3.5 - 6.5 m. Also, full soil arching formula [20] is considered.

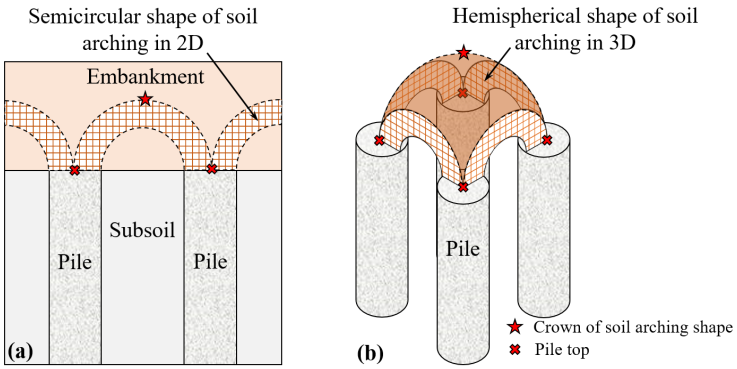

Fig. 11. Failure theory for (a) 2D plane strain and (b) 3D condition (modified from Hewlett and Randolph [19])

Table 4 is illustrated the different equations used to estimate the *SAR* in these approaches. Fig. 12 shows the variation in the results even for the same piled embankment condition. The effect of seismic excitation is not considered in these approaches. BS8006 [20] shows the higher value of the *SAR* followed by the Terzaghi [1]. Hewlett and Randolph [19] shows closely follow the numerical results. The pile spacing (s) is fixed at 2.5 m. It may due to the assumed shape of the soil arching in these design approaches. Thus, it is vital to propose a general approach for piled embankment design.

Table 4. Review of different design approaches

Design Method	**Soil arching ratio (*SAR*)**
Terzaghi [1]	$SAR = \frac{(s^2 - d^2)}{4.h.d.K.\tan\phi'}\left(1 - e^{\left(\frac{-4.h.d.K.\tan\phi'}{s^2-d^2}\right)}\right)$ where, K = (1-$\sin\phi'$)
Hewlett and Randolph [19]	**At the pile top:** $SAR = \left(\frac{1}{\left(\frac{2K_p}{K_p+1}\right)\left[\left(1-\frac{d}{s}\right)^{(1-K_p)} - \left(1-\frac{d}{s}\right)\left(1+\frac{d}{s}K_p\right)\right] + (1-\frac{d^2}{s^2})}\right)$ where, $K_p = \frac{(1+\sin\phi')}{(1-\sin\phi')}$
BS8006 [20]	**For full arching:** $SAR = \frac{2.8s}{(s+d)^2 h}\left[s^2 - d^2\left(\frac{\sigma_p}{\gamma h}\right)\right]$ where, σ_p is vertical stress on the pile

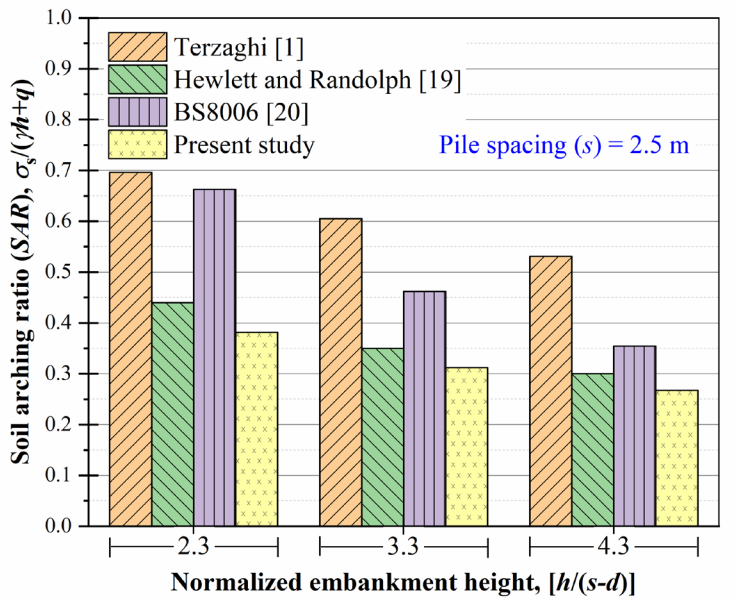

Fig. 12. Review of different design approaches for piled embankment

4 Practical implications

Followings are the practical implications of this study:

(i) It is evident that soil arching is associated with the minimum embankment height. In this study, the minimum embankment height is associated with the clear pile spacing (*s*-*d*). However, results also infer that piled embankment parameters have a significant effect on the soil arching. FEA results show that embankment modulus and effective soil friction angle are the key parameters for the mobilization of soil arching. The relationship between soil arching ratio (*SAR*), Embankment modulus (E_{em}) and effective friction angle (ϕ') is given as:

$$SAR = a.(E_{em})^2 - b.(E_{em}) + c \quad (7)$$

$$SAR = a'.(\phi')^2 - b'.\phi' + c' \quad (8)$$

where, a, b, c, a', b' and c' are empirical parameters and their values are determined as 9×10^{-4}, 4.64×10^{-2}, 8.67×10^{-1}, 2×10^{-4}, 2.16×10^{-2} and 7.63×10^{-1}, respectively. The graphical representation of these relationships are shown in Figs. 13 and 14.

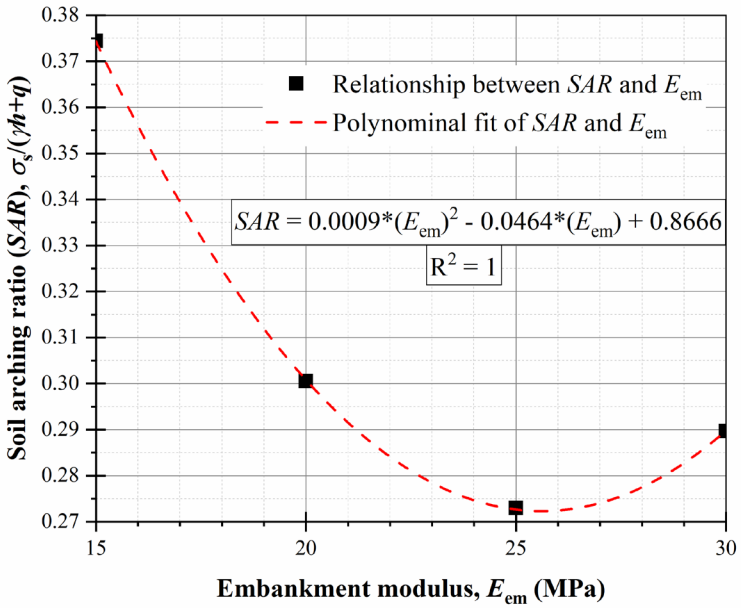

Fig. 13. Relationship between *SAR* and E_{em}

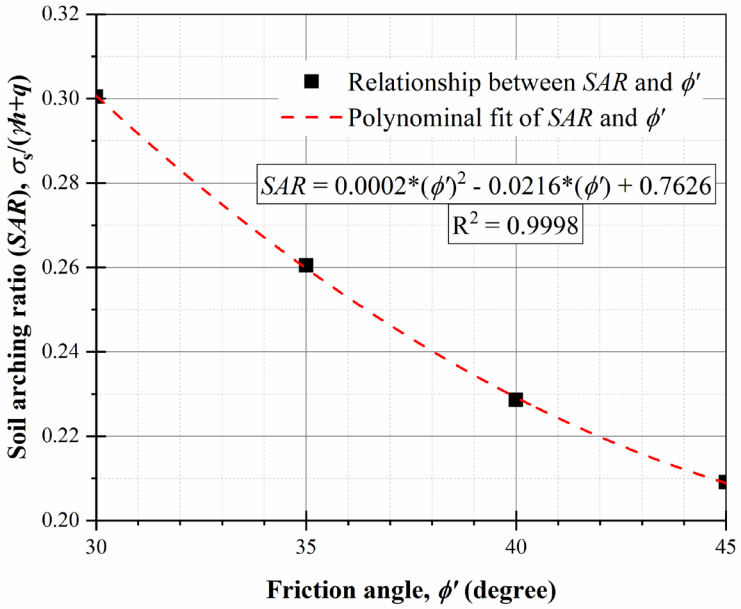

Fig. 14. Relationship between *SAR* and ϕ'

(ii) This study reports the effect of seismic excitation on the soil arching which is a crucial aspect for the piled embankment design in earthquake-prone areas and there is need of a general design approached for the

piled embankment. The mobilization partial soil arching, if not at all, is evident during seismic excitation as revealed from the numerical investigations.

Therefore, this study has practical implications to identify the key parameters of piled embankment. In addition, seismic assessment of soil arching which may lead to prevent the potential embankment failure in earthquake prone area.

5 Summary

In this study, static and seismic assessment of the soil arching mechanism in a piled embankment has been investigated under the plane strain condition. Based on the results and discussions following important findings may be summarized:

(i) The pile spacing significantly influence to the soil arching zone. The soil arching zone expands with less pile spacing. Thus, the pile spacing should be optimized to achieve the full use of soil arching.

(ii) The embankment modulus and effective soil friction angle are the key parameters for soil arching. The soil arching increase with an increase in embankment modulus and effective friction angle. Thus, the values of embankment modulus and effective friction angle should be maintained large enough to attain the full mobilization of soil arching.

(iii) The seismic excitation significantly affects the soil arching which may lead to failure of piled embankment. Thus, the seismic assessment of soil arching should be considered in the design of piled embankment.

(iv) The comparison with different design approaches reveals that current design approaches need to be improved including the seismic considerations in the piled embankment design.

References

1. Terzaghi, K.: Theoretical soil mechanics. johnwiley & sons. New York, 11-15 (1943).
2. Han, J. and Gabr, M. A.: Numerical analysis of geosynthetic-reinforced and pile-supported earth platforms over soft soil. Journal of geotechnical and geoenvironmental engineering, 128(1), 44-53 (2002).
3. Liu, H. L., Ng, C. W. and Fei, K.: Performance of a geogrid-reinforced and pile-supported highway embankment over soft clay: case study. Journal of Geotechnical and Geoenvironmental Engineering, 133(12), 1483-1493 (2007).
4. Wu, L., Jiang, G. and Ju, N.: Behavior and Numerical Evaluation of Cement-Fly Ash-Gravel Pile-Supported Embankments over Completely Decomposed Granite Soils. International Journal of Geomechanics, 19(6), 04019048 (2019).
5. Almeida, M. S. S., Fagundes, D. F., Thorel, L. and Blanc, M.: Geosynthetic-reinforced pile-embankments: numerical, analytical and centrifuge modelling. Geosynthetics International, 27(3), 301-314 (2020).
6. Heitz, C., Lüking, J. and Kempfert, H. G.: Geosynthetic reinforced and pile supported embankments under static and cyclic loading. In 4th European Geosynthetics Conference, Edinburgh, UK, 1, 1-5 (2008).

7. Lehn, J., Moormann, C. and Aschrafi, J.: Numerical investigations on the load distribution over the geogrid of a basal reinforced piled embankment under cyclic loading. Procedia engineering, 143, 435-444 (2016).
8. ABAQUS 2018, ABAQUS Documentation, Dassault Systèmes, Providence, (2018)
9. Meena, N. K., Nimbalkar, S., Fatahi, B. and Yang, G.: Effects of soil arching on behavior of pile-supported railway embankment: 2D FEM approach. Computers and Geotechnics, 123, 103601 (2020).
10. Zhang Z., Han J. and Ye G.: Numerical investigation on factors for deep-seated slope stability of stone column-supported embankments over soft clay. Engineering Geology, 168, 104-113 (2014).
11. Pham, H. V. and Dias, D.: 3D numerical modeling of a piled embankment under cyclic loading. International Journal of Geomechanics, 19(4), 04019010 (2019).
12. Potyondy J. G.: Skin friction between various soils and construction materials. Geotechnique, 11(4), 339-53 (1961).
13. Meena, N. K. and Nimbalkar, S.: Effect of water drawdown and dynamic loads on piled raft: two-dimensional finite element approach. Infrastructures, 4(4), 75 (2019).
14. USGS Earthquake Hazards Program. Available online: https://earthquake.usgs.gov/earthquakes/search/ (accessed on 6 January 2021).
15. Nimbalkar, S., Indraratna, B., Dash, S. K. and Christie, D.: Improved performance of railway ballast under impact loads using shock mats. Journal of geotechnical and geoenvironmental engineering, 138(3), 281-294 (2012).
16. Nimbalkar, S. and Indraratna, B.: Improved performance of ballasted rail track using geosynthetics and rubber shockmat. Journal of Geotechnical and Geoenvironmental Engineering, 142(8), 04016031 (2016).
17. Doyle N. F. Railway track design: a review of current practice. Canberra: Australian Government Publishing Service; 1980.
18. Jenck, O., Dias, D. and Kastner, R.: Two-dimensional physical and numerical modeling of a pile-supported earth platform over soft soil. Journal of Geotechnical and Geoenvironmental Engineering, 133(3), 295-305 (2007).
19. Hewlett, W. J. and Randolph, M. F.: Analysis of piled embankments. International Journal of Rock Mechanics and Mining Sciences and Geomechanics Abstracts, 25, 6, 297-298 (1988).
20. BS8006-1: Code of Practice for Strengthened/reinforced Soils and Other Fills. British Standards Institution, ISBN 978-0-580-53842-1 (2010).